RSC Advances

ROYAL SOCIETY OF CHEMISTRY

www.rsc.org/advances

The Bisindolylmaleimides With Anti-Parallel Conformation by N-Dodecyl Chains on Indole Rings:Thermal Property and Intensive Solid-State Fluorescence in Single Crystal

Ting-Ting Li,[a] Yong-Chen Gao,[b] Jin-Xiu Zhou, [a] Mu-Hua Huang*[a] and Yun-Jun Luo*[a]

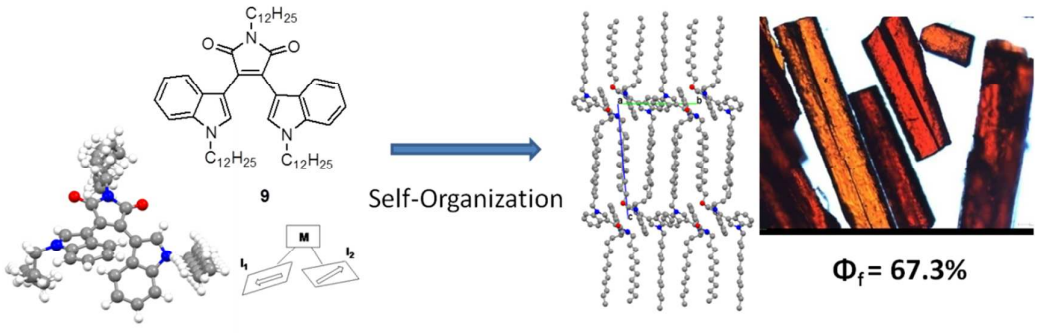

N-Dodecyl chains were located in the indole rings of BIMs to adopt anti-parallel conformation, and intensive red emission was observed in the single crystal.

Cite this: DOI: 10.1039/c0xx00000x

www.rsc.org/xxxxxx

ARTICLE TYPE

The Bisindolylmaleimides With Anti-Parallel Conformation by N-Dodecyl Chains on Indole Rings:Thermal Property and Intensive Solid-State Fluorescence in Single Crystal

Ting-Ting Li,[a] Yong-Chen Gao,[b] Jin-Xiu Zhou, [a] Mu-Hua Huang*[a] and Yun-Jun Luo*[a]

Received (in XXX, XXX) Xth XXXXXXXXX 20XX, Accepted Xth XXXXXXXXX 20XX
DOI: 10.1039/b000000x

Red emitting materials containing D(donor)-A(acceptor) system with "pyramid-mimetic" structure often gave intensive red fluorescence in the solid state. However, there's no guiding approach to fix such conformation of bisindolylmaleimides (BIMs) in solid state. In this paper, the location of N-dodecyl chains on indole rings of BIMs was found to have the "pyramid-mimetic" structure and thus gave intensive solid-state red fluorescence in the single crystal.

It's extremely significant to develop solid-state luminescence organic materials owing to their potential applications such as organic light emitting diodes (OLEDs)[1] and lasers[2]. Non-planar red emitting materials such as N-methyl-bis(4-(N-(1-naphthyl)-N-phenylamino)phenyl)maleimide (NPAMLMe)[3], 2,3-dicyano-5,6-(4'-diphenylamino-biphenyl-4-yl)-pyrazine (CAPP)[4] and bisindolylmaleimides (BIMs)[5] are promising candidates for emitting host non-doped OLEDs, since they have "pyramid-mimetic" structure to keep molecules enlarged enough to emit red light, and high emissions was kept in solid state simultaneously. Among them, BIMs are derivatives of arcyriarubins A (**1**)[6-8], a red pigment which was produced by the slime molds *Arcyria denudate*. Since arcyriarubin A (Figure 1) was isolated by Steglich[9], BIMs such as GF109203X[10] and LY333531[11, 12] have attracted much attention from pharmaceutical area owing to their biological interests.

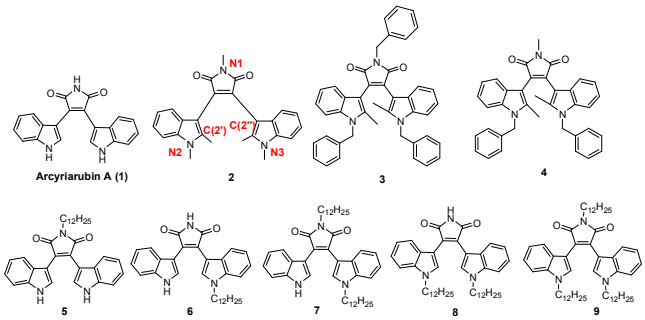

Figure 1 *N*-alkylated bisindolylmaleimides. For simplicity, the nitrogen in maleimide ring is named as *N*, the other two nitrogens in indole rings are marked as *N*2 and *N*3 respectively.

Besides, BIMs are very important in fluorescent materials development since they have D-A conjugation between indole and maleimide, as well as non-coplanarity owing to repulsion of vicinal indole rings[5, 13-16]. For instance, BIMs **2** was developed by Chow group[17] as red electroluminescence materials, the BIMs **3** and **4** have been made by Tian group[18] as non-doped red organic light-emitting materials. Interestingly, **2** and **3** showed parallel conformation for the two indole rings in solid state, but **4** showed anti-parallel conformation. It's pointed out that anti-parallel conformation (or "pyramid-mimetic" structure[5]) -the maleimide in the peak of the tower, the two indole rings as side faces and two benzyl rings as underside, which could inhibit close stacking and keep intensive solid-state luminescence. However, it is challenging to always keep the conformation as "pyramid-mimetic" structure, since there still lack well-established guidance approaches. In the case of **2**-**4**, the bulkyl substituents were put at C(2') and C(2'') positions of BIMs to keep the non-planar conformation and thus easy formation of amorphous glass in the solid state. We wonder if the introduction of long alkyl chain could tune the conformation of BIMs and their photophysical properties in the solid state through self-organization of alkyl chains[19]. In fact, the alkane chain effect[20-22] has been widely used to tune the fluorescence, solubility, thermal property and so on.

In the present work, we report the BIMs with anti-parallel conformation by the aid of the location of N-dodecyl chains on indole rings. The specific conformation of molecules will influence the thermal properties and solid-state fluorescence, especially in single crystal.

Compounds **5-8** were synthesized and characterized by us recently[23], compound **9** was synthesized in DMF by using NaH as base (see Electronic Supplementary Information). Compounds **5-9** showed good thermal stability with a weight loss of 5% over 360 □ (Figure S1 and Table S1, ESI) as estimated by thermogravimetric Analysis (TGA) measurements. Generally, the thermal stability of BIMs increased with the introduction of dodecyl chain, i.e., 361 □ for **6** , 381□ for **5**, 384 □ for **7**, 407 □ for **8** and 403 □ for **9**. It can be seen that, the symmetry of the molecule affected the thermal stability very much. For example, the symmetric **5** with N-momododecyl chain was 20 □ more thermal stable than the asymmetric **6**, and the symmetric **8** with N-didodecyl chain was 23 □ more thermal stable than asymmetric **7**.

The above compounds were also studied by differential scanning calorimetry (DSC) (Figure **2**). The sample was heated at 20 ^{o}C/min during the first scan, then cooled at the same rate followed by repeating once. From the first heating, the melting

points of **6**, **7**, **8** and **9** were measured to be 130 □, 73 □, 95 □ and 65 □ respectively. The introduction of flexible dodecyl chain generally decreased the melting points of the resulting materials, with **8** as an exception. It is believed to be its ordered organization by the aid of intermolecular H-bonding (Figure **6**).

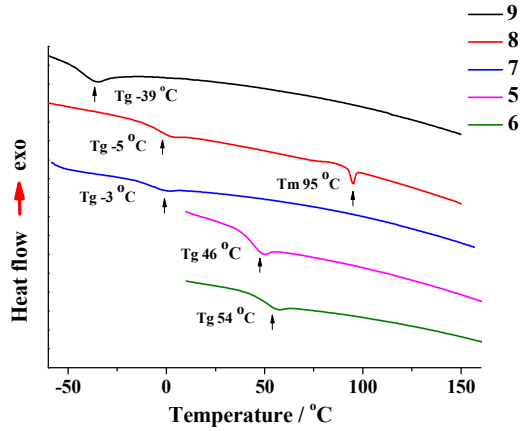

Figure 2 DSC plots of compounds **5-9** upon second heating after slow cooling

The second scan on **8** gave slow endothermic hump at -5 °C and sharp endothermic peak at 95 °C, which corresponds to glass transition temperature (Tg) and melting temperature (Tm) respectively (Fig **2**). Compared with similar BIMs with two melting points[24] such as **2** (Figure **1**), compound **8** showed only one Tm, this should be indicative of only one conformation instead of two in **8**, i.e., anti-parallel conformation. The second scans of DSC on compounds **5**, **6**, **7** and **9** exhibited no Tm, only Tg at 46, 54, -3 and -39 °C respectively (Table S**1,** ESI). The existence of Tg indicated the formation of amorphous species, which can not give crystalline or hemicrystaline during cooling. The exception of **8** among other BIMs to give Tm may be caused by its high symmetry in the molecule and intermolecular H-bonding interaction as showed in its single crystal structure (Figure **5**). With the increase of flexible dodecyl chain in the molecules, the glass transition temperature went down from 54 °C to -39 °C, owing to the motility's increase of the resulting materials.

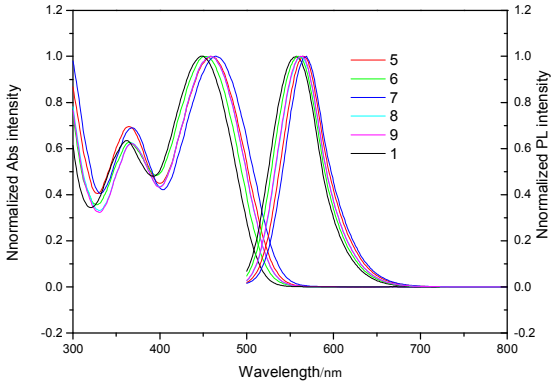

Figure 3 Normalized UV−Vis absorption and Fluorescence spectra of compound **1** and **5-9** in THF (6×10^{-5}M)

Absorption and emission spectra of **1** and **5-9** in THF were shown in Figure **3** and Table **1**. Two major absorption bands were observed, one in the visible region around 453-464 nm and one around 360-370 nm in the UV region. It might be caused by the charge transfer (CT) transitions involving both indole and maleimide moieties[25, 26]. The molar absorptivity of **1** and **5-9** are similar (log**ε** = 3.95-4.15), with the maximum absorption band of 448-464 nm. Compared to **1**, introduction of dodecyl chain showed a red shift both for maximum absorption, though in different extent (Table **1**). **7** showed the biggest shift of 16 nm for maximum absorption.

Table **1** UV-Vis and Fluorescence of compounds**1** and **5-9**

Compd[a]		Absorption λ_{max}[b]/nm (log**ε**)	Fluorescence λ_{max}[c] /nm (**Φ**f[d]/%)	Stokes shift **Δ**[b] (nm)	Life time **τ** (ns)[f]
1	THF	448 (4.08)	555 (62.7)	107	10.56
	Film[e]	483	693(0.9)	210	0.3189
5	THF	461 (3.99)	565 (54.4)	104	12.11
	Film[e]	477	648 (1.2)	171	0.5200
6	THF	453 (4.02)	560 (56.7)	107	11.73
	Film[e]	483	644 (0.9)	161	0.5476
7	THF	464 (3.95)	568 (53.2)	104	11.81
	Film[e]	486	629 (2.2)	143	4.59
8	THF	459 (4.04)	564 (70.2)	105	12.52
	Film[e]	481	622 (24.3)	141	3.66
9	THF	458 (4.15)	562 (63.7)	104	11.74
	Film[e]	475	608 (7.6)	137	1.45

[a]Photophysical properties in THF were recorded at room temperature (c = 6.0×10^{-5} M). [b]Only the longest absorption maxima are shown. [c]Exited at the longest absorption maxima for solution, and 460 nm for solid sample. [d]Absolute fluorescence quantum yield, measured using a Hamamatsu Photonics Quantaurus QY. [e]Drop-casting film prepared from a THF solution. [f]The fluorescence life time **τ** was measured using a 440 nm picoseconds pulse diode laser and the value given in nanoseconds (ns).

In the fluorescent spectra, all the samples in THF were irradiated at the longest absorption maxima, an emission at region around 562-568 nm were observed. The absolute quantum yield of 54-70% (Table **1**) was estimated for compounds **5-9**, and **8** had the highest quantum yield of 70%. The Images of the above compounds in THF solution under 365 nm UV light was shown in Figure S2 (ESI). The similar quantum yields of **1** and **5-9** could be the result of equilibration of parallel and anti-parallel conformation in diluted solution. The solvent effects on these compounds were conducted by UV-Vis and fluorescent spectra on **8** and **9**. The absorption spectra of **8** show slight red shift (λ_{max}) with the increase of solvents' polarity, with similar molar absorptivity (Figure S4 and Table S2 in ESI). The photoluminescent spectra of **8** also show red shift (λ_{max}) with the increase of solvents' polarity, but the intensity decreased with the increase of polarity of solvents (Figure S5 and Table S2 in ESI). Similar changes were seen in compound **9** towards different solvents (Figure S6, S7 and Table S3 in ESI). BIMs **8** and **9** have rather high emissions in nonpolar solvents, and lower emissions in polar solvents such as DMF and acetonitrile, only in ethanol, the emission of BIM is strongly quenched. The photographs of **8** and **9** in different solvents were shown in Figure S8 (ESI). The relative lower emissions of BIMs in polar protic solvents indicate strong solute-solvent interaction that also affect the energy level of the emitting state.

Although **1** and **5-9** showed good red fluorescence in THF solution, they had much lower quantum yields in the film (Table **1**). Their images under 365 nm UV light were shown in Figure S3. However, compared with the quantum yield as low as 0.9-2.2% for **5-7, 8** and **9** remained quantum yield as high as 24% and 7% respectively. In the normalized UV-Vis absorption of samples in

film (Figure **4**), very similar maximum absorption at ca. 480 nm was see. While the max emission wavelength of film samples moved to short wavelength with the introduction of N-dodecyl chain. The arcyriarubin A (**1**) gave fluorescence at 677 nm, N-monododecyl product of **5** and **6** gave 649 and 645 nm respectively, N,N-didodecyl products of **7** and **8** gave 629 and 625 nm, and tridodecyl product of **9** gave 608 nm (Table **1**).

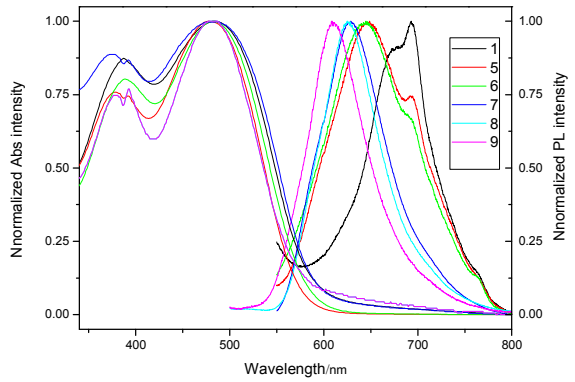

Figure 4 Normalized UV−Vis absorption and Fluorescence spectra of compounds **1** and **5-9** in film (exited at 460 nm)

The Fluorescent life time of materials is an important parameter and has been utilized to new applications[27]. All the samples was measured and listed in Table **1**. The life time of all the samples in THF was in the range of 10-13 ns, while 0.3-4.6 ns for the samples in film. And the solvents did not influence the life time so much in the case of compound **8** (see Figure S13and Table S4 in ESI).

It is known that aggregation patterns as well as morphology of dye molecules can govern their photophysical properties in the solid state. Encouraged by the fluorescence of **8** and **9** based on the film sample, we further investigated their crystal structures and solid-state fluorescence in more details. The single crystals of **8** and **9** were obtained by slow evaporation of petroleum ether and ethyl acetate, which were suitable for X-ray diffraction measurement. The crystal data were shown in Table **2**.

Table **2** Crystal data collection for **8** and **9**

Parameters	Compound **8**	Compound **9**
CCDC deposit number	1003005	1404958
Empirical formula	$C_{44}H_{61}N_3O_2$	$C_{56}H_{79}N_3O_2$
Formula weight	663.96	832.29
Temperature/K	102.3	113
Crystal system	triclinic	triclinic
Space group	P-1	P-1
a/Å	11.2782(9)	11.246(2)
b/Å	11.2830(9)	12.502(3)
c/Å	15.7258(13)	18.736(4)
α/°	88.215(7)	83.75(3)
β/°	79.997(7)	74.78(3)
γ/°	83.701(7)	85.12(3)
Volume/Å^3	1958.7(3)	2522.3(9)
Z	2	2
ρ_{calc}g/cm^3	1.126	1.088
Radiation	Mo Kα (λ = 0.7107)	Mo Kα (λ = 0.7107)

Compound **8** crystallizes in a triclinic P-1 space group. Its crystal structure determination revealed that the two indole rings are not coplanar with the ring of maleimide. This results from the steric hindrance between the indole rings, which are twisted with respect to the maleimide ring (Fig. **5a**), as already observed in other BIMs compounds[24, 28]. Interestingly, the two indole rings adopt an anti-parallel conformation, and the two dodecyl chains oriented away from the BIMs core. In the solid state of **8**, molecules are connected by pairs of N−H···O=C hydrogen bonds to form inversion dimers (Fig. **5b**), which generated $R^2_2(8)$ rings[29]. Although H-bond mediated $R^2_2(8)$ rings are very popular for carboxylic acid[30], it is rare for imides[31] or maleimides[32], especially for BIMs. The intermolecular H-bonding made **8** pack in the solid state to have head-to-head connection via imide, and the two indoles rings and dodecyl chains self-organized together in a back-to-back fashion via intermolecular interaction (Figure **6a**). The detailed π–π interaction inside the two indole rings is shown in Figure **6b**.

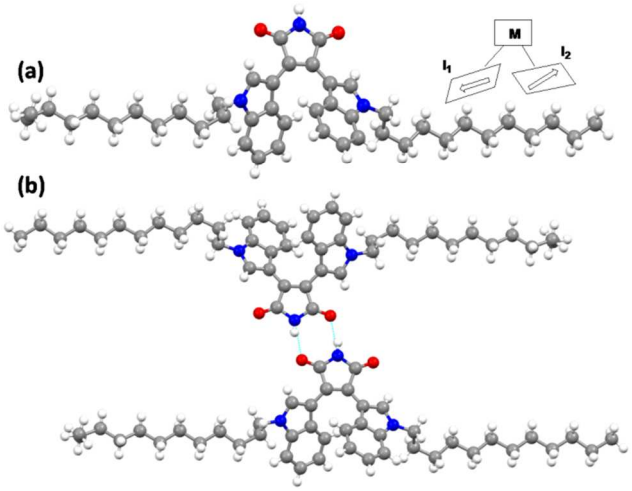

Figure **5** (a) The X-Ray determined molecule structures of **8**. The sketch righ to diagram depict the molecular structures. The arrows in the right sketches indicate the direction from the benzene ring to pyrrole in indole substituent. (b) The $R^2_2(8)$ inversion dimer through H-bond in **8**.

Inside the 8-membered ring, H1 to O1 distance amounts 2.017(1) Å, N1 to O1 distances 2.847 Å. The bond angle of O···H−N amounts 161.8°, which is close to the ideal 180°. In addition, molecule **8** could also pack into a herringbone-like structure with the alternating left-handed and right-handed configuration molecules by C-H…π interaction (Fig. **6b**).

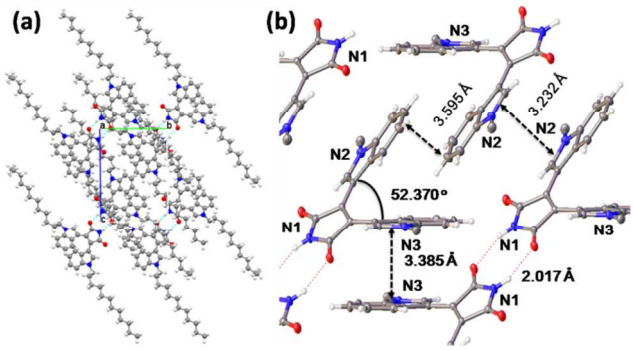

Figure **6** Crystal packing patterns of **8**. (a) The a-axis view of crystal packing of **8**. (b) The detailed packing structure of **8**, N-dodecyl groups were removed for clarity of BIMs core.

The dihedral angle of N2-indole ring and N3-indole ring amounts 52.37°. The neighbouring N2-indole rings are anti-parallel to each

other, the centroid-to-plane distance of one N2-indole ring with the neighbouring two N2-indole rings are measured to be 3.595 Å and 3.232 Å. However, these interactions can be deemed poor π–π interaction because of the centroid distance and sliding angle were 5.463 Å and 41.2°. Similarly, the neighbouring N3-indole rings are also anti-parallel to each other, with centroid-to-plane distance of 3.385 Å, and the centroid distance and sliding angle of 5.688 Å and 38.3 ° respectively. These values are too large to form strong π–π interaction[33], and may be related to the quantum yield of 44.7% in the solid state (Table **3**).

Compound **9** crystallizes in a triclinic P-1 space group too, the non-planarity and anti-parallel conformation of two indole rings was seen clearly in its crystal structure (Figure **7**).

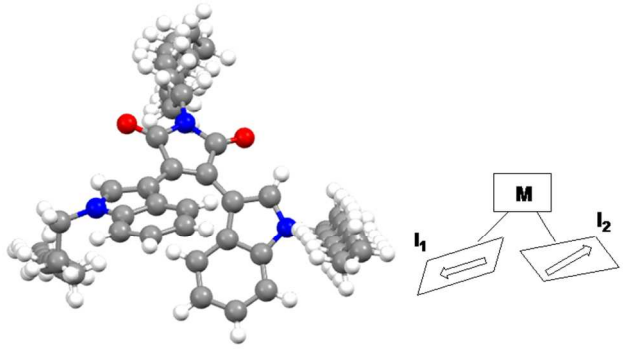

Figure **7** The X-Ray determined molecule structures of **9**. The sketch righ to diagram depict the molecular structures. The arrows in the right sketches indicate the direction from the benzene ring to pyrrole in indole substituent.

The dihedral angles between two indole rings of **9** amounts 50.8 ° which is supersimilar to **8**. Instead of the intermolecular H-bonding in **8**, the maleimide rings adopt a weak anti-parallel intermolecular interaction, giving centroid-to-plane distance of 3.31 Å, and plane centroid-plane centroid distance of 3.73 Å.

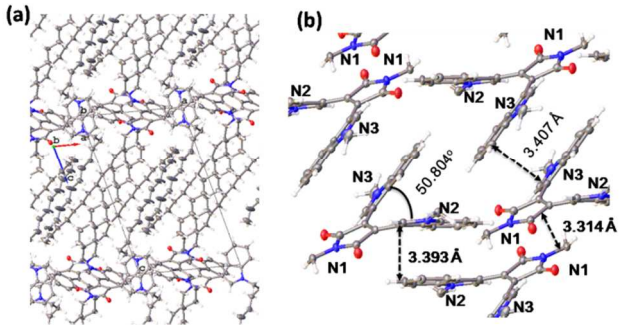

Figure **8** Crystal packing patterns of **9**. (a) The b-axis view of crystal packing of **9**. (b) The detailed packing structure of **9**, N-dodecyl groups were removed for clarity of BIMs core.

The neighbouring N2-indole rings are anti-parallel to each other, the centroid-to-plane distance of one N2-indole ring with the neighboring N2-indole ring amounts to be 3.39 Å, and plane centroid-plane centroid distance of 4.03 Å. The corresponding value for N3-indole rings is 3.41 Å and 4.83 Å. Clearly, these values are too large to form strong π–π interaction[33], and may be related to the quantum yield of 67.3% in the solid state. The higher quantum yield of **9** than **8** is believed to be the looser stacking of molecules and thus weaker intermolecular interaction, which reduce the fluorescence quenching in more extent.

Compared with the highly ordered packing in single crystals, the regularity of microcrystal powder and film samples decrease, which should reduce the emission efficiency in the solid state. Indeed, the photographs of three different samples were recorded by a microscope (Figure **9**). Red column crystals were observed in the single crystal of **8**. While in the powder sample of **8**, the irregular small crystals could still be seen, and red lotus leaf-like film was shown in the drop-casting sample. In the single crystal of **9**, the more regular but smaller rod-like crystal was seen than that of **8**. In the powder sample of **9**, less and irregular crytals were seen compared to that of **8**. In the drop-casting film, the fiber-like film was observed.

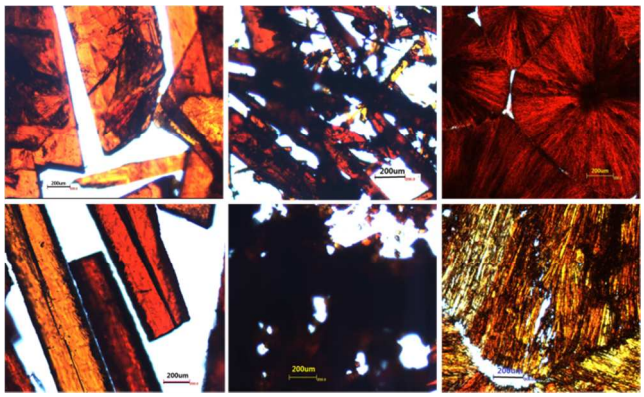

Figure **9** Microscopic photographs of **8**-single crystal, **8**-powder, **8**-film (up) and **9**-single crystal, **9**-powder and **9**-film (down).

The absolute quantum yields of the samples were measured and shown in Table **3**. For compound **8**, since the intermolecular H-bonding will aid the crystallization, hence the differences between three samples became very small, 26.4% for film sample, 43.1% for powder sample, and 44.7% for single crystal sample. That may imply the ordered packing will contribute to the emissions in the solid state. As far as **9** is concerned, it is not as easy as **8** to crystallize, which can be observed during DSC measurement. The big differences was seen among film sample, powder sample and single crystal sample, i.e., absolute quantum yield of 8.1%, 14.2% and 67.3% respectively.

Table **3** The solid-state fluorescence of **8** and **9** in different forms

Sample	λ_{max}em (nm)	Φ_f[a]/%
8-crystal	641	44.7
8-powder	637	43.1
8-film	622	26.4
9-crystal	615	67.3
9-powder	610	14.2
9-film	608	8.1

[d]Absolute fluorescence quantum yield, measured using a Hamamatsu Photonics Quantaurus QY

In conclusion, the N-dodecyl chain was introduced to locate in the indole rings to adopt anti-parallel conformation of BIMs in the solid state, which in turn adjust the corresponding thermal behaviour and solid-state fluorescence. Although all BIMs were found to have intensive fluorescence in solution, only **8** and **9** were found to be fluorescence active in film, owing to the anti-parallel conformation of two indole rings to inhibit close stacking. The more orderly stacked single crystal of **8** and **9** showed solid-state fluorescence as high as 43% and 67% respectively. The small difference of solid-state fluorescence among film, powder and single crystal sample of **8** could be caused by the easy crystallization of **8** owing to the intermolecular hydrogen bond mediated $R^2_2(8)$ inversion dimer, which also explained the

melting point of 95 °C upon second heating in DSC measurement. The more detailed investigation on the single crystals of BIMs is ongoing in our lab, which will be reported in the due course.

The authors thank The National Natural Science Foundation of China (No. 21202008) and Beijing Institute of Technology (Excellent Young Researcher Fund 2012YR0910) for generous support. Prof Zhong H.-Z. and Prof. Dong Y.-P. are thanked for inspiring discussions, Mr. Zhou Q.-C. was thanked for his help for measuring fluorescence spectra.

Notes and references

[a] *School of Materials Science and Engineering, Beijing Institute of Technology, Beijing, 100081, China. Fax: 0086-10-68911608; Tel: 0086-10-68911608;E-mail: mhhuang@bit.edu.cn, yjluo@bit.edu.cn.*

[b] *College of Chemistry and Molecular Engineering, Zhengzhou University, Zhengzhou, 450052 China.*

† Electronic Supplementary Information (ESI) available: The TGA, solution absorption, PL spectra and photographs of **5-9** under 365 nm. See DOI: 10.1039/b000000x

1. H. Uoyama, K. Goushi, K. Shizu, H. Nomura and C. Adachi, *Nature*, 2012, **492**, 234-238.
2. S. Kena-Cohen and S. R. Forrest, *Nat. Photonics*, 2010, **4**, 371-375.
3. W. Wu, H. Yeh, L. Chan and C. Chen, *Adv. Mater.*, 2002, **14**, 1072-1075.
4. S. Chen, X. Xu, Y. Liu, G. Yu, X. Sun, W. Qiu, Y. Ma and D. Zhu, *Adv. Funct. Mater.*, 2005, **15**, 1541-1546.
5. Z. Ning, Y. Zhou, Q. Zhang, D. Ma, J. Zhang and H. Tian, *J. Photochem. Photobiol., A*, 2007, **192**, 8-16.
6. M. Brenner, H. Rexhausen, B. Steffan and W. Steglich, *Tetrahedron*, 1988, **44**, 2887-2892.
7. K. Kamata, T. Suetsugu, Y. Yamamoto, M. Hayashi, K. Komiyama and M. Ishibashi, *J. Nat. Prod.*, 2006, **69**, 1252-1254.
8. P. D. Davis, L. H. Elliott, W. Harris, C. H. Hill, S. A. Hurst, E. Keech, M. K. H. Kumar, G. Lawton, J. S. Nixon and S. E. Wilkinson, *J. Med. Chem.*, 1992, **35**, 994-1001.
9. W. Steglich, B. Steffan, L. Kopanski and G. Eckhardt, *Angew. Chem.*, 1980, **92**, 463-464.
10. S. Roy, A. Eastman and G. W. Gribble, *Org. Biomol. Chem.*, 2006, **4**, 3228-3234.
11. M. M. Faul, L. L. Winneroski, C. A. Krumrich, K. A. Sullivan, J. R. Gillig, D. A. Neel, C. J. Rito and M. R. Jirousek, *J. Org. Chem.*, 1998, **63**, 1961-1973.
12. B. M. Trost and W. Tang, *Org. Lett.*, 2001, **3**, 3409-3411.
13. T. Yeh, T. J. Chow, S. Tsai, C. Chiu and C. Zhao, *Chem. Mater.*, 2006, **18**, 832-839.
14. Y. P. Huang, S. Tsai, D. Huang, T. Tsai and T. J. Chow, *React. Funct. Polym.*, 2007, **67**, 986-998.
15. Y. Li, L. Cao, Z. Ning, Z. Huang, Y. Cao and H. Tian, *Tetrahedron Lett.*, 2007, **48**, 975-978.
16. Z. Lin, Y. Wen and T. J. Chow, *J. Mater. Chem.*, 2009, **19**, 5141-5148.
17. C. Chiu, T. J. Chow, C. Chuen, H. Lin and Y. Tao, *Chem. Mater.*, 2003, **15**, 4527-4532.
18. Z. Lin, Y. Lin, C. Wu, P. Chow, C. Sun and T. J. Chow, *Macromolecules*, 2010, **43**, 5925-5931.
19. K. Liu, F. Qiu, C. Yang, R. Tang, Y. Fu, S. Han, X. Zhuang, Y. Mai, F. Zhang and X. Feng, *Cryst. Growth Des.*, 2015, **15**, 3332-3338.
20. H. Li, S. S. Babu, S. T. Turner, D. Neher, M. J. Hollamby, T. Seki, S. Yagai, Y. Deguchi, H. Moehwald and T. Nakanishi, *J. Mater. Chem. C*, 2013, **1**, 1943-1951.
21. N. Koumura, Z. Wang, S. Mori, M. Miyashita, E. Suzuki and K. Hara, *J. Am. Chem. Soc.*, 2006, **128**, 14256-14257.
22. J. Mei and Z. Bao, *Chem. Mater.*, 2014, **26**, 604-615.
23. Y. Gao, Y. Jia, T. Li, Z. Hei, F. Yang, M. Huang and Y. Luo, *ARKIVOC*, 2015, **(5)**, 153-163.
24. C. Chiu, T. J. Chow, C. Chuen, H. Lin and Y. Tao, *Chem. Mater.*, 2003, **15**, 4527-4532.
25. K. Saita, M. Nakazono, K. Zaitsu, S. Nanbu and H. Sekiya, *J. Phys. Chem. A*, 2009, **113**, 8213-8220.
26. Z. Lin, Y. Wen and T. J. Chow, *J. Mater. Chem.*, 2009, **19**, 5141-5148.
27. A. Saha, Z. Panos, T. Hanna, K. Huang, M. Hernandez-Rivera and A. A. Marti, *Angewandte Chemie, International Edition*, 2013, **52**, 12615-12618.
28. Z. Ning, Y. Zhou, Q. Zhang, D. Ma, J. Zhang and H. Tian, *J. Photochem. Photobiol., A*, 2007, **192**, 8-16.
29. G. R. Desiraju, *Angew. Chem. Int. Ed.*, 1995, **34**, 2311-2327.
30. J. Bernstein, R. E. Davis, L. Shimoni and N. Chang, *Angew. Chem. Int. Ed.*, 1995, **34**, 1555-1573.
31. A. T. Hulme, A. Johnston, A. J. Florence, P. Fernandes, K. Shankland, C. T. Bedford, G. W. A. Welch, G. Sadiq, D. A. Haynes, W. D. S. Motherwell, D. A. Tocher and S. L. Price, *J. Am. Chem. Soc.*, 2007, **129**, 3649-3657.
32. M. H. K. Ebbing, M. Villa, J. Valpuesta, P. Prados and J. De Mendoza, *Proc. Natl. Acad. Sci.*, 2002, **99**, 4962-4966.
33. H. Xi, C. Yuan, Y. Li, Y. Liu and X. Tao, *CrystEngComm*, 2012, **14**, 2087-2093.